REPORT DOCUMENTATION PAGE

Form Approved
OMB No. 0704-0188

1. REPORT DATE *(DD-MM-YYYY)*	2. REPORT TYPE	3. DATES COVERED *(From - To)*
May 2004	Journal Article Reprint	2004

4. TITLE AND SUBTITLE
Activated Carbon Fiber Cloth Electrothermal Swing Adsorption System

5a. CONTRACT NUMBER

5b. GRANT NUMBER

5c. PROGRAM ELEMENT NUMBER
106013

6. AUTHOR(S)
Patrick D. Sullivan, mark J. Rood, Georges Grevillot, Joseph D. Wander and K. James Hay

5d. PROJECT NUMBER

5e. TASK NUMBER

5f. WORK UNIT NUMBER
ARMT0052

7. PERFORMING ORGANIZATION NAME(S) AND ADDRESS(ES)
University of Illinois

8. PERFORMING ORGANIZATION REPORT NUMBER

9. SPONSORING/MONITORING AGENCY NAME(S) AND ADDRESS(ES)
Air Force Research Laboratory
Airbase Technologies Division
139 Barnes Drive, Suite 2
Tyndall AFB FL 32403-5323

10. SPONSOR/MONITOR'S ACRONYM(S)

11. SPONSOR/MONITOR'S REPORT NUMBER(S)
AFRL-ML-TY-TP-2004-4538

12. DISTRIBUTION/AVAILABILITY STATEMENT
Distribution Statement "A". Distribution Unlimited

13. SUPPLEMENTARY NOTES
Published in Environmental Science & Technology, Vol 38 (2004), pp 4865-4877

14. ABSTRACT

Capture and recovery of hazardous air pollutants (HAPs) and volatile organic compounds (VOCs) from gas streams using physical adsorption onto activated carbon fiber cloth (ACFC) is demonstrated on the bench-scale. This system is regenerated electrothermally, by passing an electric current directly through the ACFC. The adsorbate desorbs from the ACFC, rapidly condenses on the inside walls of the adsorber, and then drains from the adsorber as a pure liquid. Rapid electrothermal desorption exhibits such unique characteristics as extremely low purge gas flow rate, rapid rate of ADFC heating, rapid mass transfer kinetics inherent to ACFC, and in-vessel condensation. An existing system was scaled up 500%, and the new system was modeled using material and energy balances. ... These results allow the modeling of electrothermal desorption of organic vapors from gas streams with in-vessel condensation to optimize operating conditions of the system during regeneration of the adsorbent.

15. SUBJECT TERMS

16. SECURITY CLASSIFICATION OF:			17. LIMITATION OF ABSTRACT	18. NUMBER OF PAGES	19a. NAME OF RESPONSIBLE PERSON
a. REPORT	b. ABSTRACT	c. THIS PAGE			Patrick Sullivan
U	U	U	SAR	13	19b. TELEPHONE NUMBER *(Include area code)* 850-283-0430

Environ. Sci. Technol. 2004, 38, 4865–4877

Activated Carbon Fiber Cloth Electrothermal Swing Adsorption System

PATRICK D. SULLIVAN* AND MARK J. ROOD*

Department of Civil and Environmental Engineering, University of Illinois, Urbana, Illinois 61801

GEORGES GREVILLOT

Chemical Engineering Science Laboratory–CNRS, ENSIC, Nancy 54001, France

JOSEPH D. WANDER

United States Air Force Research Laboratory, Tyndall AFB, Florida 32403

K. JAMES HAY

U.S. Army Engineer Research and Development Center–CERL, Champaign, Illinois 61826-9005

Capture and recovery of hazardous air pollutants (HAPs) and volatile organic compounds (VOCs) from gas streams using physical adsorption onto activated carbon fiber cloth (ACFC) is demonstrated on the bench-scale. This system is regenerated electrothermally, by passing an electric current directly through the ACFC. The adsorbate desorbs from the ACFC, rapidly condenses on the inside walls of the adsorber, and then drains from the adsorber as a pure liquid. Rapid electrothermal desorption exhibits such unique characteristics as extremely low purge gas flow rate, rapid rate of ACFC heating, rapid mass transfer kinetics inherent to ACFC, and in-vessel condensation. An existing system was scaled up 500%, and the new system was modeled using material and energy balances. Adsorption isotherms using methyl ethyl ketone (MEK) and ACFC were obtained while electricity passed through the ACFC and at temperatures above MEK's boiling point. These isotherms agreed within 7% to Dubinin–Radushkevich modeled isotherms that were extrapolated from independently determined gravimetric measurements obtained at lower temperatures. Energy and material balances for the electrothermal desorption of organic vapors and ACFC agree to within 7% of experimentally measured values. These results allow the modeling of electrothermal desorption of organic vapors from gas streams with in-vessel condensation to optimize operating conditions of the system during regeneration of the adsorbent.

Introduction

Traditional methods used to regenerate activated carbon adsorbents and capture adsorbed hazardous air pollutants/volatile organic compounds (HAPs/VOCs) include vacuum and thermal treatments. Thermal treatments include steam, heating with an inert purge gas, and heating with close-proximity electrically resistive elements. Steam is the commonest method to regenerate carbonaceous adsorbents (*1*).

Alternative techniques to thermally regenerate carbonaceous adsorbents include direct electrical heating, inductive electrical heating, and microwave heating (*2*). These techniques offer distinct advantages over the more traditional adsorbent regeneration techniques:

(i) Energy efficiency is higher than heating by steam or inert gas because the energy is delivered directly to the adsorbent and adsorbate, thus minimizing the energy expended to heat the vessel and ancillary equipment.

(ii) Heating rate of the adsorbent is not limited by heat/mass transfer rates between the carrier gas and the adsorbent because the energy is directly applied to the adsorbent and adsorbate rather than being delivered by the carrier gas stream.

(iii) Effluent concentration of adsorbate can be maximized because the purge gas flow rate is controlled independent of the rate of heating of the adsorbent.

(iv) Unlike steam regeneration, direct heating techniques do not contaminate the system with water, which is difficult and costly to separate from water-miscible adsorbates, and can cause corrosion.

(v) Equipment needed to regenerate the adsorbent is much simpler and more compact than traditional techniques.

Of the techniques that apply energy to the adsorbent internally, direct electrical heating or electrothermal desorption (ED) is the most promising. For example, inductive regeneration has technical difficulties in evenly distributing the energy throughout the adsorbent and from energy losses in the transmission of energy to the adsorbent from the source of power. Electrothermal desorption energy efficiency has been verified by modeling (*3*). Additional references on ED of carbonaceous adsorbents are found in Sullivan (*4*). Much recent ED activity has been in France (*5–7*) and at University of Illinois (*8, 9*).

Rapid ED of ACFC, with in-vessel condensation of the adsorbate, was demonstrated at the bench-scale with an automated dual-vessel system (*4, 10*). The system was developed to remove methyl ethyl ketone (MEK) from air, which is difficult to accomplish with traditional granular activated carbon (GAC) because of the occurrence of bed fires (*11, 12*). This was the first successful system to continuously capture dilute organic vapors from air and recover liquid adsorbate using electrothermal-swing adsorption (ESA) in a fixed-bed system without a separate condensation unit (*4*).

The objectives of this study are to advance ACFC/ESA technology by developing, demonstrating, and modeling the energy and material balances for a larger bench-scale system. To model the ED portion of ESA, equilibrium data for the elevated temperatures and concentrations experienced during desorption were needed. This research characterizes the applicability of the Dubinin–Radushkevich (DR) equation to describe the equilibrium partitioning of organic vapor between the gas and solid phases at conditions experienced during ED. The new bench-scale adsorber is 500% larger than the previous ACFC/ED system (*13*). This new design also represents a practical and more simplified configuration for further scale-up. A new ED model is developed to characterize the dominant parameters controlling ED and to describe the electrical energy consumed and the condensate recovered during regeneration. This model is also

* Authors to whom correspondence may be addressed. E-mail: patrick.sullivan@tyndall.af.mil (P.D.S.); mrood@uiuc.edu (M.J.R.).

10.1021/es0306415 CCC: $27.50
Published on Web 08/06/2004

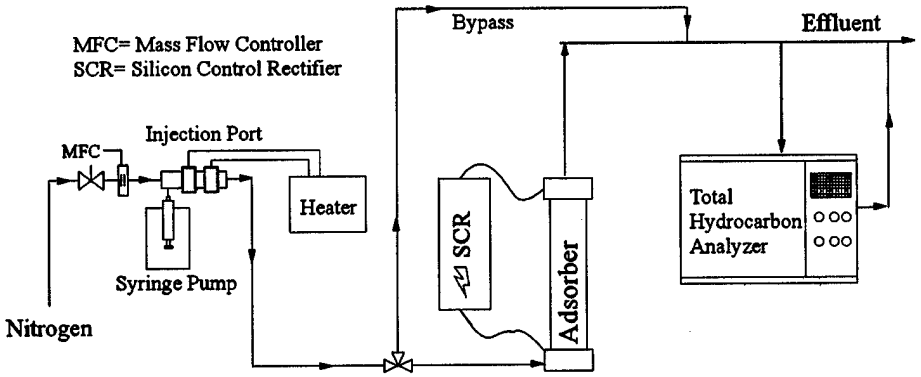

FIGURE 1. Schematic of system used to produce adsorption isotherms.

used to predict energy requirements for select ED operating conditions.

Experimental Apparatus and Methodology

Adsorption Isotherms. The experimental system used to obtain the high-temperature adsorption isotherm data consisted of a gas generation unit, the adsorption vessel, a direct electrical heating power supply, and a gas detection unit (*4*). The gas generation unit used laboratory-grade N_2(g) as the carrier gas, and it was metered with a mass flow controller (Tylan, model FC-280) upstream of the vessel. Liquid adsorbate was delivered to the N_2(g) steam through an injection port using a syringe pump (KD Scientific, model KDS200) and hypodermic needle. The injection port contained 0.9 g of ACFC (American Kynol Inc., type ACC-5092-20; *14*) configured into a wick attached to the end of the hypodermic needle to buffer fluctuations in feed rate of the liquid adsorbate. The port was heated to ~100 °C with externally clamped-on electrical resistance heaters to enhance evaporation (see Figure 1).

The cylindrical portion of the adsorption vessel was made of Pyrex, with an outer diameter of 75 mm and a wall thickness of 4 mm. The vessel contained 37.45 g of ACFC (American Kynol Inc., type ACC-5092-20). The ACFC was rolled into a hollow cylinder with an inner diameter of 19 mm. The ACFC was heated during the breakthrough tests by passing alternating electrical current through the fabric. Thermocouples (Omega Inc., Type K) were positioned on the inner and outer surfaces of the ACFC cartridge to monitor the temperature of the adsorbent. The thermocouples were ungrounded and electrically isolated with an electrically protected thermocouple module (Keithley, model MB47-K-05) because the thermocouples were in contact with the ACFC as electrical current passed through the ACFC. Total gas flow rates during these breakthrough tests were 10−12 standard L/min. The bed was regenerated between runs by increasing the ACFC's temperature to 250 °C while purging the vessel with ultrahigh-purity (UHP) N_2(g). Direct electrical heating was applied to the ACFC with a silicon control rectifier (SCR) (Robicon, series 440) using alternating current. Effluent concentration of the adsorber was measured by a total hydrocarbon analyzer using flame ionization detection (THC/FID, MSA/Baseline Inc., series 8800).

The high-temperature isotherms that were obtained while electrical current passed through the ACFC were completed with the use of breakthrough tests. Results from these tests described the adsorption capacity of the ACFC at select inlet concentrations of organic vapor as described by:

$$W = \frac{P_{tot}(MW)Q_{air}}{\rho_l m_s RT}\int_0^{t_{sat}}\left(\frac{Y_{in}}{1-Y_{in}} - \frac{Y_{out}}{1-Y_{out}}\right)dt \quad (1)$$

where W is the volume of adsorbed organic vapor per unit mass of adsorbent, P_{tot} is the total pressure of the inlet gas stream, MW is the molecular weight of the adsorbate, Q_{air} is the volume flow rate of carrier gas, R is the ideal gas constant, T is the absolute temperature of the inlet carrier gas, m_s is the mass of the adsorbent, ρ_l is the bulk liquid density of the adsorbate, Y_{in} is the mole fraction of adsorbate in the inlet gas stream, Y_{out} is the mole fraction of adsorbate in the exhaust gas stream, and t_{sat} is the time at which Y_{out} has reached its final, steady-state value because the adsorbent is saturated with respect to the adsorbate.

The DR equation, which is based on volume pore filling for microporous adsorbents, has been shown to accurately describe the equilibrium relationship between the gas and solid phases for ACFC adsorbent tested here at 293 K ≤ T ≤ 323 K (*15*–*17*). The Wagner equation is used here to determine the saturation vapor pressure of the adsorbate (*18*).

Electrothermal Swing Adsorption Tests. The bench-scale ACFC/ESA system, along with the ancillary equipment, is shown in Figure 2. The gas generation system was the same system as used for the high-temperature isotherm tests described above, except that air was used as the carrier gas instead of N_2(g) during adsorption, N_2(g) was used as the purge gas during regeneration, and a mixing vessel was added downstream of the injection port to increase the uniformity of the organic vapor concentration at the higher gas flow rates used for the adsorption cycles. A flask beneath the adsorber collected condensate draining from the vessel during the desorption tests. A standard laboratory top-loading gravimetric balance recorded the mass of condensate collected over time, to be compared with results from the desorption model.

This adsorber was scaled up 500% from its predecessor (*4*). This new adsorber contains four cartridges to increase the total adsorption capacity per unit vessel volume, decreased amount of wettable inner surface area of the adsorption vessel per unit mass of material adsorbed to the adsorbent, increased electrical resistance, and reduced system pressure drop. The vessel was 125 mm in outer diameter with 4 mm wall thickness. Gas flows during adsorption and desorption as well as the flow of electrical current during desorption are also described in Figure 3. Each of the four cartridges of ACFC had an inner diameter of 1.9 cm and a length of 20.3 cm. Total mass of the ACFC in the adsorber was 128 g.

The gas flow rate during adsorption cycles was carefully controlled at a constant value between 25 and 60 standard L/min, and adsorbate concentrations ranged from constant values of 250 to 1000 ppmv. N_2(g) gas purge rate during desorption was 1 standard L/min. Temperatures, condensate mass, and true root-mean-squared (rms) amperage and voltage were measured and recorded during desorption.

Desorption Modeling Methodology. Adsorbate is drawn from the airstream into the ACFC as the air passes through

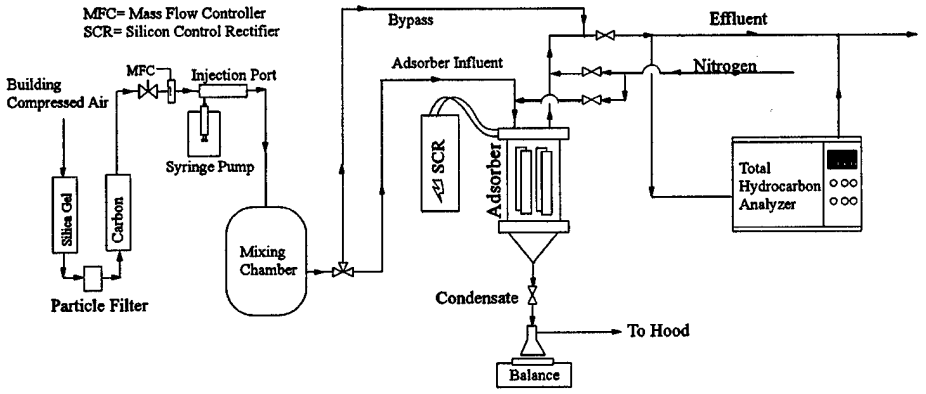

FIGURE 2. Schematic of ESA system with 125-mm o.d. vessel used to collect mass and energy balance information.

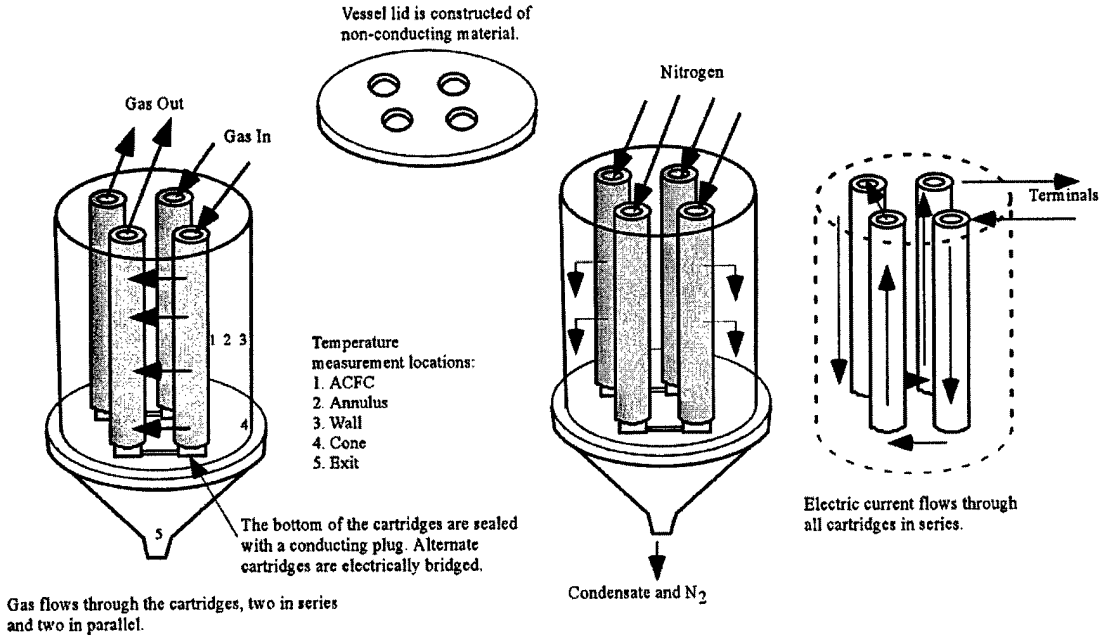

FIGURE 3. Schematic of 125-mm o.d. adsorption vessel describing gas flow during adsorption and the gas flow and electric current flow during regeneration.

multiple layers of ACFC in each cartridge. The purified airstream then exits the vessel. The ACFC must be regenerated once the adsorbate breaks through the ACFC. At that time, the air flow is turned off, and N_2(g) passes through the vessel to purge it of O_2. The ACFC's electrical resistivity allows the material to be heated by passing current through the ACFC cartridges. The fibers heat quickly (~1 °C/s) causing rapid desorption of the adsorbate (~0.5 g/s) from the ACFC. This vapor is then transported from the ACFC cartridge to the cool inner wall of the vessel, upon which condensation occurs. The condensate flows to the bottom of the vessel by gravity and exits the vessel with the N_2(g).

This idealized desorption cycle of ACFC is represented on an isotherm plot as presented in Figure 4, where the ACFC was saturated with MEK at 1000 ppmv. Point 1 represents the equilibrium adsorption capacity of the ACFC when saturated at 1000 ppmv MEK. The path from point 1 to point 2 represents the initial application of electrical power to the ACFC causing it to increase to 125 °C, and the concomitant increase in vapor concentration until the gas is saturated at the temperature of the vessel's wall. W decreases only slightly during this stage, as the mass required to saturate the annular space is 1% of the adsorbed mass of MEK. The path from point 2 to point 3 represents the second stage of adsorbent heating. The temperature of the ACFC continues to rise from 125 to 200 °C, but the vapor in the annulus remains at its saturation vapor pressure (e.g., ~0.1 atm for MEK) because the additional MEK that is released during this stage is condensed rapidly onto the interior wall of the vessel. The path from point 3 to point 4 represents the cooling stage, after the electrical power is turned off and condensed MEK has drained from the vessel. Point 4 represents the residual MEK left in the ACFC upon completion of the desorption cycle.

The following assumptions were made in modeling the desorption cycle:

(i) The ACFC is treated as an annular monolith with uniform resistivity. Such assumption is valid because the surface temperature of the ACFC was measured at 150 ± 5 °C along the entire length of the cartridge's external surface during constant power applications.

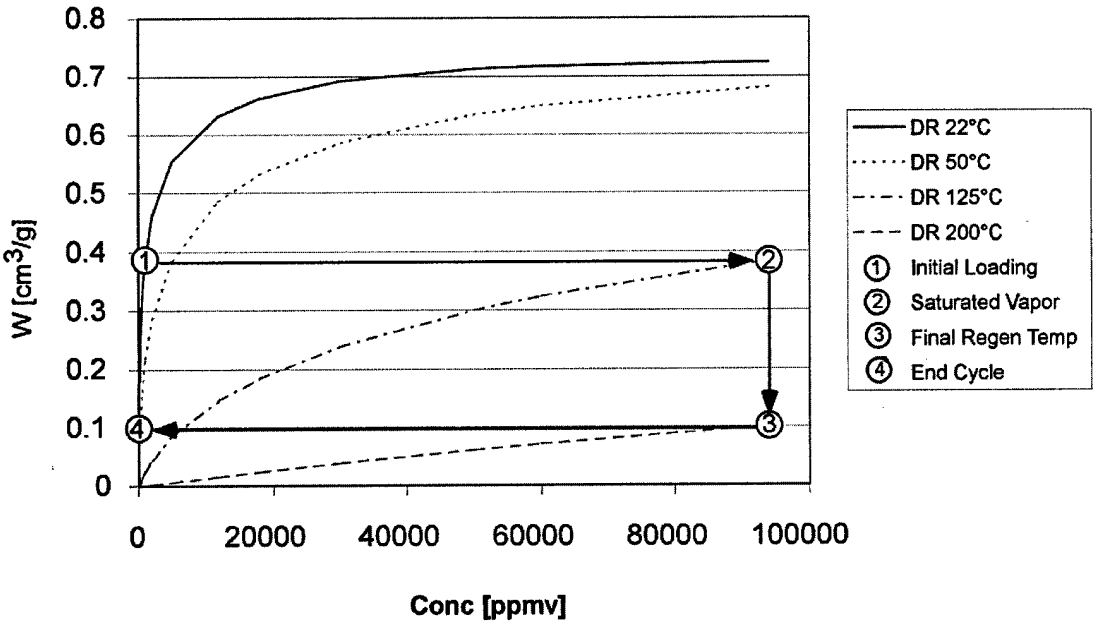

FIGURE 4. Idealized desorption process for a MEK–ACFC system represented on a series of isotherm plots.

(ii) Vapor concentration at the bulk gas–ACFC interface is in equilibrium with the adsorbed phase during electrothermal regeneration. The individual ACFC fibers are 10 ± 1 μm in diameter (*8*), which provides a large surface-area-to-mass ratio, yielding very rapid heat and mass transfer. Such assumption is also based on dimensionless breakthrough curves that exhibit the same curve structure at gas flow rates of 5–60 standard L/min and adsorbate concentration ranges from 250 to 4300 ppmv (*4*). It was also demonstrated with a polymer bead/microwave vapor recovery system that the system's desorption performance is governed by the temperature of the adsorbent and its adsorption isotherm, with insignificant influence of mass-transfer resistance during regeneration of the adsorbent (*19*). The ACFC/ED system is similar to the polymer/microwave system in that it also has rapid internal heating of the adsorbent and uses an adsorbent material that exhibits rapid mass transfer. Temperature and the adsorption isotherm are the dominant factors that define desorption of the ACFC/ED system.

(iii) Concentration of vapor in the annular space between the ACFC and the vessel shell is uniform. The distance between the adsorbent and the vessel shell is 0.5–1 cm. At this distance, molecular diffusion alone would provide mass transport of the adsorbate across the annular space on a time scale of ~5 s. The computations are made with a time-step of 1 s, so other effects must contribute to the annular mixing. Buoyancy-driven convection provides additional dispersion of the adsorbate within the annulus. Although detailed computational fluid dynamics (CFD) modeling of this free-convection mixing is beyond the scope of this effort, preliminary results indicate substantial mixing on a 1-s time scale in the later part of the cycle. A third effect contributes to the transport of the adsorbate from the ACFC to the vessel shell. Once the condensation commences, the resulting volume reduction at the point of condensation creates bulk convection toward the vessel shell. When purge gas is used, additional bulk convection results. The transport of the adsorbate from the ACFC toward the vessel shell is a complex combination of these four factors, and the magnitude of their combined effect supports the mixing assumption for the annular space.

(iv) Condensation of vapor on the vessel's wall is instantaneous. Dropwise condensation was observed for the adsorbates tested here. Therefore, the rate of condensation for these adsorbates at the internal surface of the vessel's wall was modeled to be ~ 8 mL/s based on dropwise condensation (*20*). However, the peak release rate from the ACFC is ~ 0.5 mL/s, based on the temperature of the adsorbent and the adsorption isotherm. Therefore, the condensation rate at the wall of the vessel is not limiting the rate of liquification of the vapor. The vapor that is desorbed from the ACFC rapidly condenses on the vessel's inner wall once the annular space is saturated with respect to the vapor's concentration at the temperature of the vessel's wall.

(v) A vertical desorption wave travels through a small portion of the bed when a purge gas is used. The length of the mass transfer zone within this desorption wave is negligible. It is observed experimentally that desorption runs performed with or without N_2(g) purge gas are nearly indistinguishable from each other during the application of electrical power. Specifically the final temperature, energy consumption, and total mass of adsorbate recovered for a desorption run without purge gas are all within 5% of the values obtained from tests with the same applied power and 1 standard L/min of N_2(g). The mass of vapor carried by the purge gas is ~3% of the total adsorbed mass of MEK. When purge gas is used, the volume is sufficient for a desorption wave to penetrate no more than 10% of the depth of the bed. Ignoring the thickness of the mass transfer zone during desorption introduces a small error in modeling the desorption cycle while dramatically simplifying the computations.

Energy and material balances can be constructed with the boundary of the control volume along the inner surface of the adsorption vessel (inner dashed line of Figure 5). The material balance describes the amount of condensate formed by considering the decrease in the adsorbate mass loading in the adsorbent (W), the increase in the vapor concentration in the annulus, and the flow from the vessel of vapor that is in the purge gas (eq 2, Figure 6).

$$\frac{dm_l}{dt} = \rho_l m_s \frac{dW}{dt} - \frac{P_{tot} V M_W}{RT} \frac{dY}{dt} - \frac{Q_g t P M_W Y}{RT} \qquad (2)$$

where dm_l is the change in condensate mass within the control volume, W is the volume of adsorbate per mass of

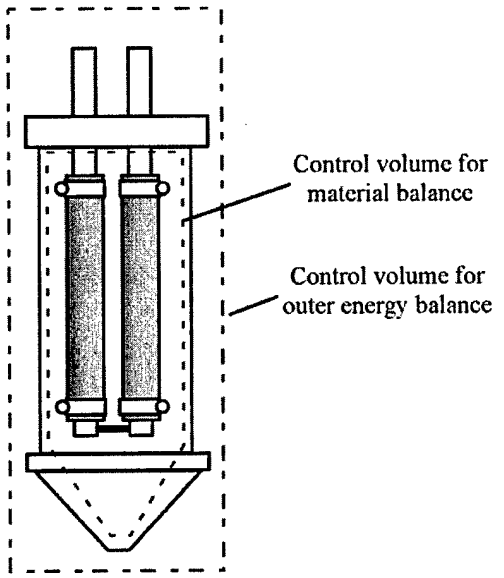

FIGURE 5. Schematic of 125-mm diameter adsorber showing control volumes for the inner and outer mass and energy balances.

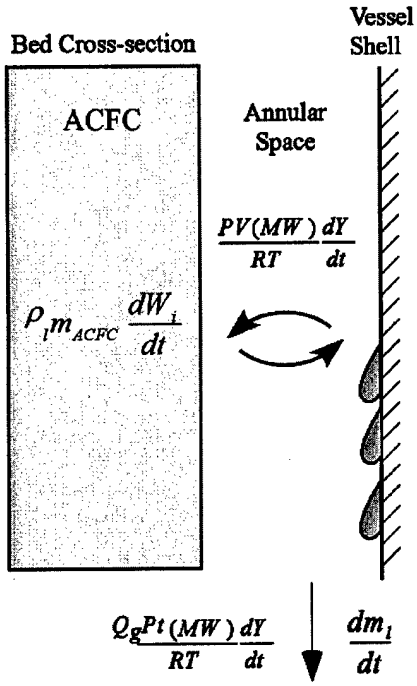

FIGURE 6. Conceptual diagram of desorption mass balance.

adsorbent, P_{tot} is the total pressure in the vessel, V is the volume of the vessel, M_W is the molecular weight of the adsorbate, R is the ideal gas constant, T is the absolute temperature, Y is the mole fraction of adsorbate in the gas, t is time, and Q_g is the total volume flow rate of the purge gas.

The bulk gas-phase concentration within the vessel is computed knowing the mass of material adsorbed on the ACFC and the adsorbent's temperature by combining the DR equation and Wagner's equation (*13*):

$$Y=\frac{P_c \exp\left[\left(\frac{VP_A x+VP_B x^{1.5}+VP_C x^3+VP_D x^6}{1-x}\right)\right]}{P_{tot}\exp[E_i\sqrt{-\ln(W/W_o)}/RT]} \quad (3)$$

where P_c is the critical pressure; VP_A, VP_B, VP_C, and VP_D are Wagner constants for the adsorbate, $x=1-(T/T_c)$; T_c is the critical temperature of the adsorbate, W is the volume of adsorbate per mass of adsorbent, W_o is the micropore volume per unit mass of adsorbent, and E is the adsorption energy of the adsorbate. The temperature of the ACFC is needed to determine the equilibrium vapor concentration at the ACFC-gas/vapor interface, and the resulting mass flow rate of condensate from the ACFC (eq 2). A combined mass and energy balance is used to determine the temperature of the ACFC. The electrical energy input is equated to the product of the heat of adsorption and the change in adsorbate loading plus the summation of the heat capacities times the change in temperature terms, plus the conductive, convective, and radiative losses of the ACFC as developed for the inner energy balance of Figure 5 and described schematically in Figure 7 and analytically in eq 4:

$$VI=m_s\Delta H_{ads}\frac{dq}{dt}+\sum m_f c_{pf}\frac{dT}{dt}+m_s(c_{ps}+qc_{pl}+(q_o-q)c_{pv})\frac{dT}{dt}+Q_g c_{pg}\frac{dT}{dt}+hA_{conv}(T-T_\infty)+\epsilon\sigma A_{rad}(T^4-T_\infty^4)+\frac{kA_{cond}}{L}(T-T_\infty) \quad (4)$$

where m_s is the mass of the solid (adsorbent); H_{ads} is the heat of adsorption; $q=\rho_l W$ where W is the volume of adsorbate per mass of adsorbent; m_f is the mass of the adsorber's components in direct contact with the adsorbent; c_p values are the mass-specific heat capacities for the adsorber's materials (c_{pf}), the adsorbent (c_{ps}), liquid adsorbate (c_{pl}), and gas-phase adsorbate (c_{pv}); Q_g is the mass flow rate of the gas; h is the convective heat transfer coefficient at the ACFC interface; T is the temperature of the ACFC; ϵ is the emissivity of the ACFC; σ is the Stefan–Boltzmann constant; A_{conv}, A_{rad}, and A_{cond} are the effective surface areas for convection, radiation, and conduction, respectively; k is the thermal conductivity coefficient of the stainless steel tubing into and out of the vessel; L is the length of conduction along the stainless tubing; V is rms voltage; and I is rms current. A detailed list of the parameters used in eq 4 with example adsorbate values for MEK is provided in Table 1.

A second energy balance along the outer boundary of the entire adsorber (Figure 5) is also performed for closure. Conductive losses across the polypropylene gas supply and exhaust tubes are neglected, as the temperatures of the N_2(g) stream at the vessel's inlet and outlet connections are within 5 °C of ambient conditions, and the estimated conduction through the polypropylene tubing connected to the adsorber is less than 1% of the total energy input. An energy term for the condensation of the adsorbate (ΔH_{vap}) is added since the adsorbate crosses the boundary as a liquid:

$$VI=m_s\Delta H_{ads}\frac{dq}{dt}+\sum m_f c_{pf}\frac{dT}{dt}+m_s(c_{ps}+qc_{pl}+(q_o-q)c_{pv})\frac{dT}{dt}+Q_g c_{pg}\frac{dT}{dt}+hA_{conv}(T-T_\infty)+\epsilon\sigma A_{rad}(T^4-T_\infty^4)-\Delta H_{vap}\frac{dm_l}{dt}+\frac{kA_{cond}}{L}(T-T_\infty) \quad (5)$$

An average heat capacity of graphitic carbon was used for the ACFC, since no data are available for ACFC. The ambient temperature (20 °C) was used for T_∞ in the radiation calculations. The error in the radiation energy term introduced by neglecting the radiation back from the vessel shell to the ACFC is calculated to be <10% of the radiation term.

Electrical resistivity of the ACFC ($\rho(T)$) decreases with increasing temperature as described by:

$$\rho(T)=\rho_R(1+\alpha(T-T_R)) \quad (6)$$

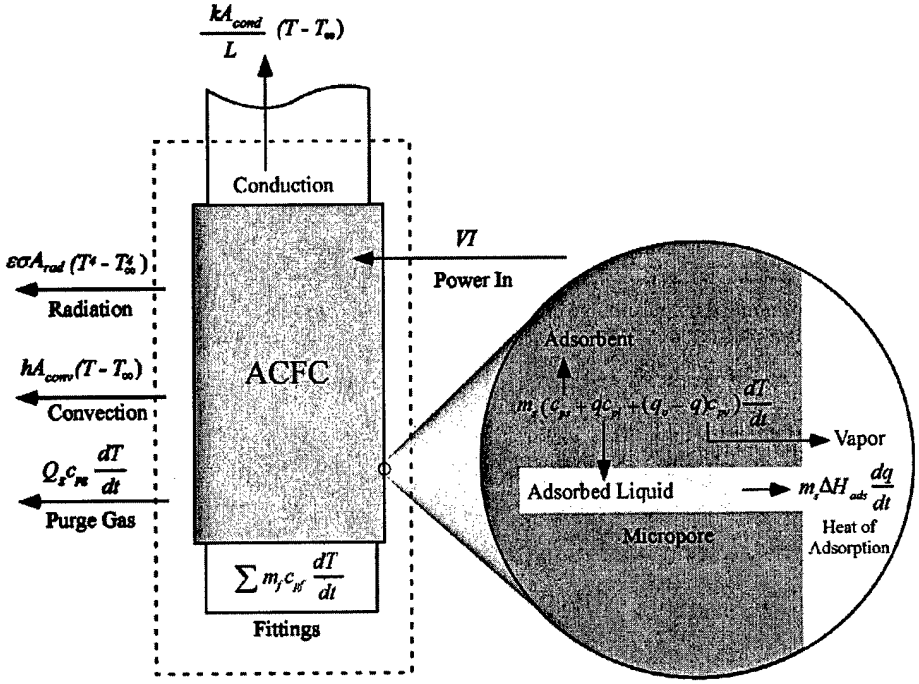

FIGURE 7. Energy balance diagram.

TABLE 1. Input Parameters for Desorption Modeling

variable description	symbol	value	units	source
mass of adsorbent	m_s	128	g	measured
heat of adsorption	H_{ads}	917.9	J/g	*21*
loading, adsorbate/ACFC	q	0.0–0.6	g/g	computed from DR eq
heat capacity (aluminum)	c_{pf}	0.9	J g^{-1} K^{-1}	*22*
heat capacity (304 stainless)	c_{pf}	0.468	J g^{-1} K^{-1}	*20*
heat capacity (ACFC)	c_{ps}	0.71	J g^{-1} K^{-1}	*20*
heat capacity (MEK(l))	c_{pl}	2.19	J g^{-1} K^{-1}	*18*
heat capacity (MEK(g))	c_{pv}	1.4	J g^{-1} K^{-1}	*18*
heat capacity (N_2(g))	c_{pg}	1.04	J g^{-1} K^{-1}	*22*
total micropore volume	W_o	0.748	cm^3/g	*21*
adsorption potential	E	14.43	kJ/mol	*21*
emissivity	ϵ	0.9	N/A	*20*
Stefan–Boltzmann constant	s	5.67E−8	W/m^2·K^4	*20*
area for conduction	A_{cond}	8.12E−4	m^2	measured
area for convection	A_{conv}	0.13	m^2	calculated by SEM[a]
area for radiation	A_{rad}	0.13	m^2	calculated by SEM
length of conduction	L	0.038	m	measured
cond heat transfer coeff	k	15	W m^{-2} K^{-1}	*20*
conv heat transfer coeff	h	$f(T)$	W m^{-2} K^{-1}	*20*
mass of fittings (aluminum)	m_f	69	g	measured
mass of fittings (stainless)	m_f	262.3	g	measured
liquid density	ρ_l	0.81	g/mL	*22*
N_2(g) flow rate	Q_g	0 or 1	standard L/min	measured
power input function	$f(I,t)$	I = 9.8	A	measured

[a] SEM, scanning electron micrograph.

where ρ_R is the resistivity of the ACFC at T_R and α is the thermal resistivity factor of the ACFC. α for the Kynol-based ACFC has been measured at -3.0×10^{-3} °C^{-1} (*9*).

Since the purge gas volume is relatively low (or zero), the primary mechanism for convective heat transfer from the ACFC is free convection in the annular space. The convective heat transfer coefficient for convection of thermal energy from the ACFC to the gas in the annular space is estimated using (*20*)

$$h = \frac{Nu_L k}{L} \tag{7}$$

$$Nu_L = \left\{0.825 + \frac{0.387 Ra_L^{1/6}}{[1 + (0.492/Pr)^{9/16}]^{8/27}}\right\}^2 \tag{8}$$

$$Ra_L = \frac{g\beta(T_s - T_\infty)L^3}{\eta\nu} \tag{9}$$

where h is the convective heat transfer coefficient, Nu_L is the Nusselt number, k is the thermal conductivity for the gas, L is the vertical length of the heat transfer surface, Ra_L is the Rayleigh number, Pr is the Prandtl number, g is the constant of gravity, β is the reciprocal of the film temperature (average of T_s and T_∞), T_s is the surface temperature of the heat transfer

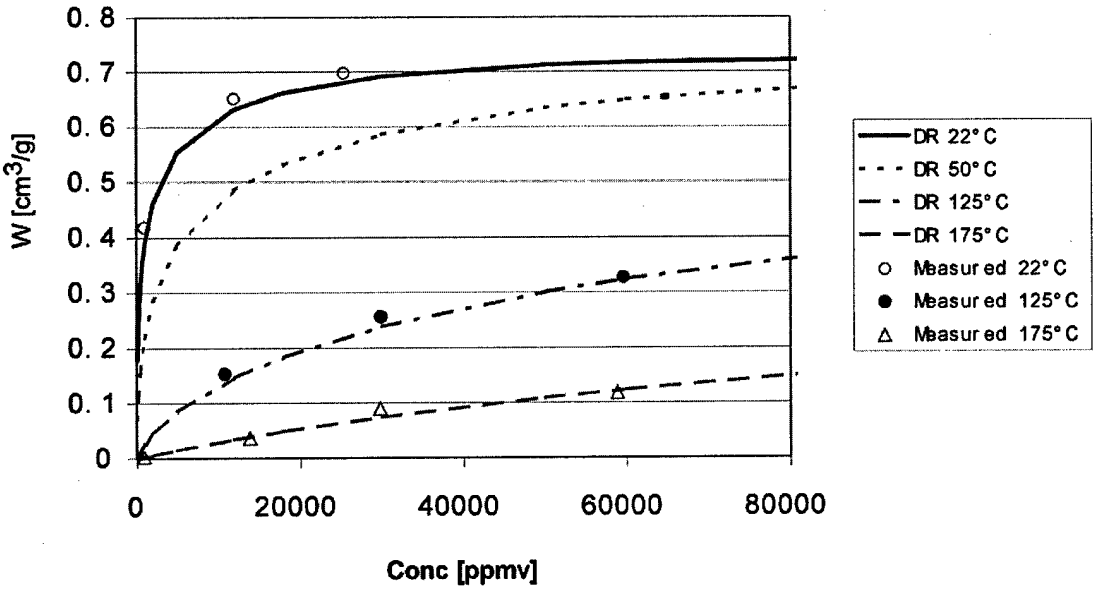

FIGURE 8. Measured MEK adsorption capacities obtained with breakthrough curves and electrothermal heating (symbols) and modeled isotherms (lines) based on the DR equation with gravimetric data and indirect heating (*21*).

surface, T_∞ is the ambient temperature, η is the thermal diffusivity, and ν is kinematic gas viscosity.

The outer surface area of the ACFC cartridges is used in the convection and radiation calculations. The vertical surface area of a smooth cylinder representing an ACFC cartridge would have an area (A) equal to πDH. The woven ACFC surface however is textured.

Scanning electron micrographs (*14*) were used to approximate the ACFC surface area. A photograph of the profile-view of the ACFC surface was placed in a computer graphics program, and the surface was traced at the detail level of the yarn bundles that are just discernible with the naked eye. This tracing formed the basis for quantifying a value of $2A$ as the effective surface area for use in heat transfer calculations involving the ACFC.

Combining the mass balance, equilibrium expression, and energy balance that are described in eqs 2−4, respectively, yields a single equation for T as a function of t as the only variable. The temperature of the adsorbent and the release rate of adsorbate throughout the desorption cycle can then be computed given the applied power input function to the system, $f(V,t)$ or $f(I,t)$ that is included in eq 4. This system of equations was solved by finite difference using Matlab with a 1-s time interval.

During the initial phase of desorption, the first term in eq 2 can be ignored as there is no condensation, and the increase in the vapor concentration will be equal to the decrease in adsorbent loading. Because the mass of the adsorbate needed to saturate the annular space is ~1% of the total adsorbed mass, the calculation can be simplified by assuming W_l to be constant, allowing C to be computed directly as a function of temperature. After the concentration reaches the saturation vapor pressure, any additional adsorbate released will condense and drain from the vessel. The third term in eq 2 becomes constant, as the concentration in the annulus remains at P_s during condensation. The resulting one-dimensional nonadiabatic model, with in-vessel condensation, accounts for all the dominant energy and mass transfer mechanisms needed to characterize the ED process.

Results and Discussion

Adsorption Isotherms. Measured adsorption capacities using the high-temperature adsorption isotherm system are plotted as symbols and the lines represent results from the DR equation, with coefficients derived by Ramirez et al. (W_{lo} = 0.748 cm^3/g, E = 14.43 kJ/mol, Figure 8) (*21*). The 22 and 50 °C isotherm lines were derived from the independent gravimetric system while the 125 and 175 °C lines result from extrapolating the DR equation obtained at the lower temperatures.

Data obtained with breakthrough curves at 22 °C are within 3.1% of the values predicted by the DR equation (*21*). Adsorption capacity data obtained when ACFC is heated directly with electricity and indirectly with inert gas agree within 7.1% for the 125 and 175 °C tests. These results indicate that the DR equation can be used to model the equilibrium partitioning of MEK vapor between the bulk gas and adsorbent throughout the temperature and concentration ranges experienced during electrothermal regeneration of the ACFC, even at temperatures above MEK's boiling point.

Desorption Temperature Measurements. The dependence of temperature for specific locations within the adsorber during the application of electrical power to the ACFC is described in Figure 9. Voltage was adjusted with a feedback control loop receiving an input signal from a temperature sensor in combination with eq 6 to maintain a constant current of ~10 A for 200 s. The ACFC did not contain adsorbate for this test, and N_2 purge gas flowed through the ACFC at 1 standard L/min. Locations for all of the thermocouples are as depicted in Figure 3. In contrast to the isotherm measurements, the thermocouple characterizing the ACFC's surface temperature during regeneration was located 2 mm from its surface to protect the instrumentation from electrical current. Note that the thermocouple located 2 mm from the interior glass wall of the vessel heated to 120 °C while the aluminum collection cone remained <30 °C, and the gas exiting the system remains within 2 °C of ambient temperature when no adsorbate is present.

The test described in Figure 9 was repeated, except the ACFC was initially saturated with 1000 ppmv of MEK in dry air, and the N_2 gas flowed trough the vessel at 1 standard L/min (Figure 10). Higher temperatures for the thermocouple locations near the vessel exit were observed during this test. Heat of condensation most likely played a role in heating of the thermocouples. More time is required to reach the final temperature at constant current when the ACFC contains adsorbate, because additional energy is required to desorb

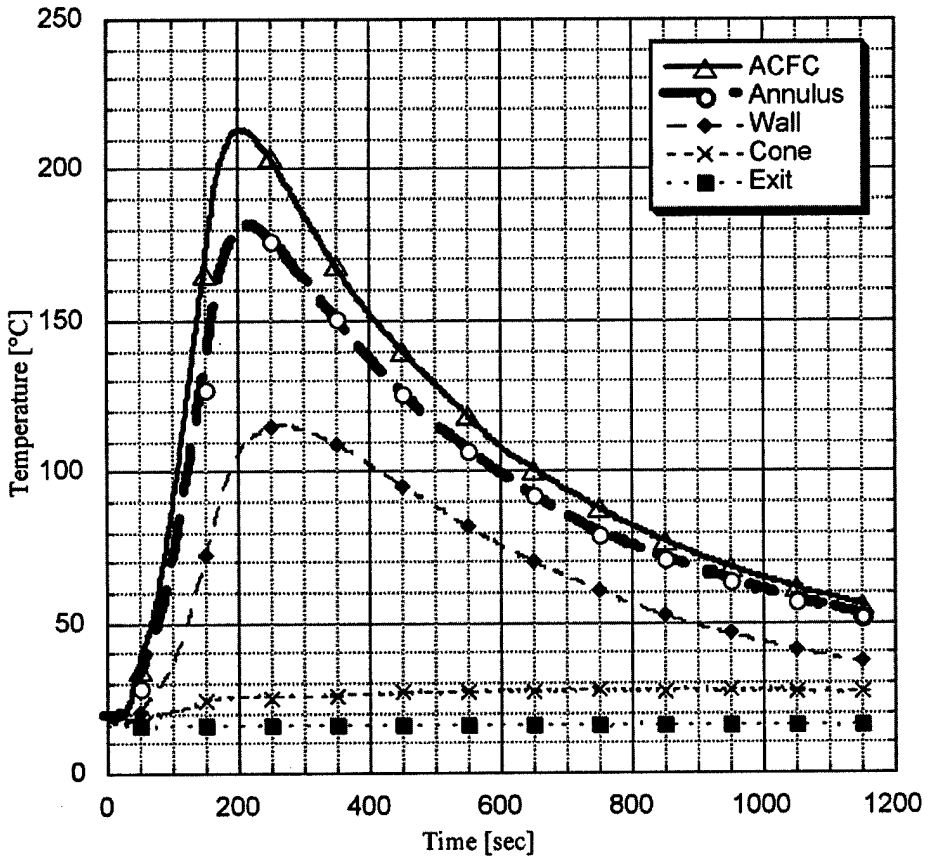

FIGURE 9. Measured temperature profiles for heating and then cooling at select locations within the adsorber, without adsorbate present.

the adsorbate. The amount of time that power is applied during desorption increased from ~200 to ~300 s, indicating that a significant portion of the energy is required to desorb the adsorbate. Mass of desorbed MEK is plotted on the secondary axis of Figure 10. The formation of the condensate coincides with a sudden increase in the temperatures at the cone and exit locations. The exit temperature is within 20 °C of ambient temperature and supports the assumption that a majority of the adsorbate is condensed within the adsorber before it exits the vessel.

Energy Balances. Closures for the energy balances were evaluated by comparing the experimentally measured electrical energy consumed to regenerate a saturated adsorbent to the energy required to heat the adsorbent when considering the inner and outer energy balances (eqs 4 and 5, respectively). As previously mentioned, N_2 gas flow was 1 standard L/min for all regeneration tests. The total energy input was obtained by integrating the measured voltage and current readings during the experiment. The measured temperature profiles were then combined with the energy balances and numerically integrated to describe the energy required to heat the system. The inner and outer energy balances provided closure within −7% and +2% of the measured energy input values, respectively (Figures 11 and 12). These closures are reasonable when considering the limited number of temperature measurement locations and that 10-s time steps were used in computing the energy losses from the measured temperature data. The inner energy balance indicates that radiation from the ACFC consumes 13% of the energy input, and the adsorber can be improved by using a reflective inner wall of the vessel.

Results from combined mass and energy balance modeling were then compared with measured results to compare the spatial and temporal deposition of energy within the adsorber during electrothermal desorption of adsorbate (Figure 13). This adsorbent was initially saturated at 1000 ppmv MEK. The overall heat capacity term in Figure 13 includes all of the heat capacities within the adsorber as described by eq 4. The electrical current was kept constant at 9.8 A (standard deviation = 0.081, $n = 27$). During the first 40 s, the majority of the electrical energy (~85%) heats the ACFC and the liquid adsorbate with 15% of the energy lost to conduction, convection, and radiation. As the vapor concentration reaches the bulk gas saturation value, the adsorbate is rapidly released and initially consumes 40% of the energy deposited to the adsorber between 40 and 50 s. The conductive, convective, and radiative losses gradually increase as the system heats. The total modeled energy usage agrees within 3.2% with the measured cumulative electrical energy input (dashed line).

Adsorbate Recovery Results. The temporal variability of modeled and measured cumulative mass fractions of MEK condensate for a desorption cycle, with current maintained at 9.8 A is provided in Figure 14. The cumulative mass of MEK condensate collected from the vessel is shown in panel A, and the ACFC's temperature is described in panel B. The modeled results in panel A were shifted 20 s to compensate for the delay in capture of the liquid MEK in the gravimetric balance as observed in Figure 2. The modeled and measured temperatures deviate significantly from each other. The measured temperature is linear and lags when compared to the modeled temperature. The thermocouple is 2 mm away from the ACFC's surface causing inefficient heat transfer between the ACFC and thermocouple because of the low specific heat of air that is transferring heat from the ACFC to the thermocouple. There is also a lag in sensing temperature changes by the thermocouple because it is encased in a stainless steel sheath. Visual observation of the time when

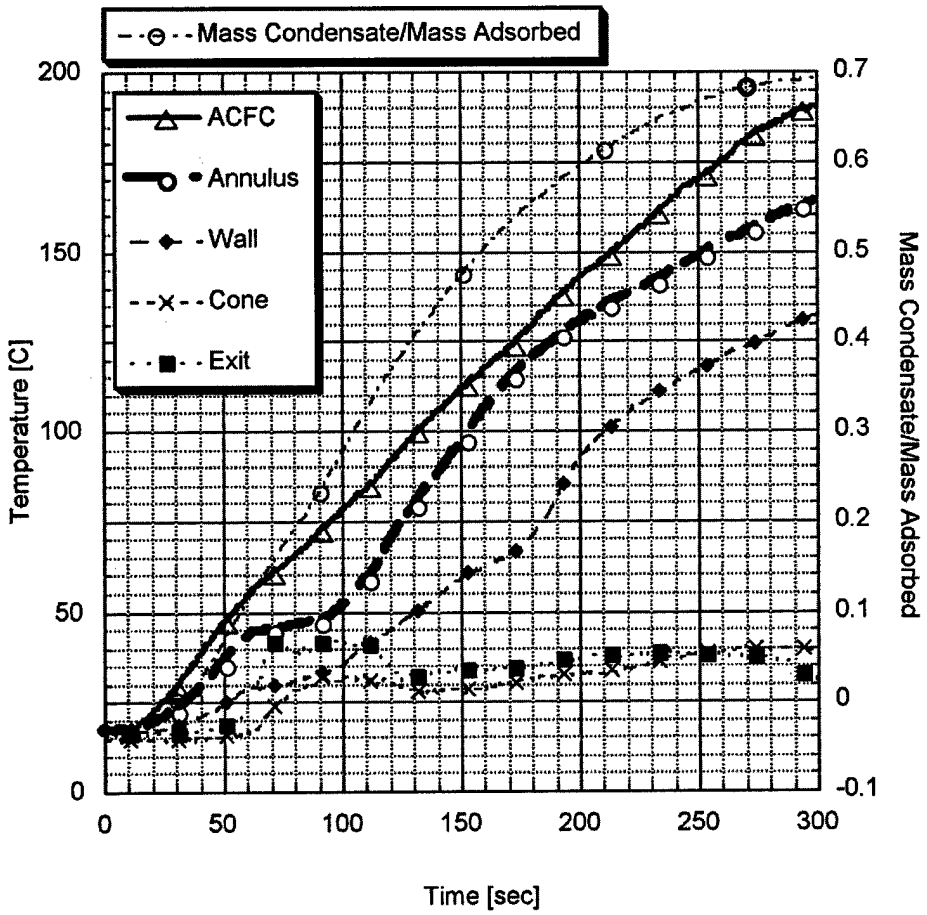

FIGURE 10. Measured temperature profiles for heating at select locations within the adsorber during desorption of MEK and cumulative mass of collected MEK condensate.

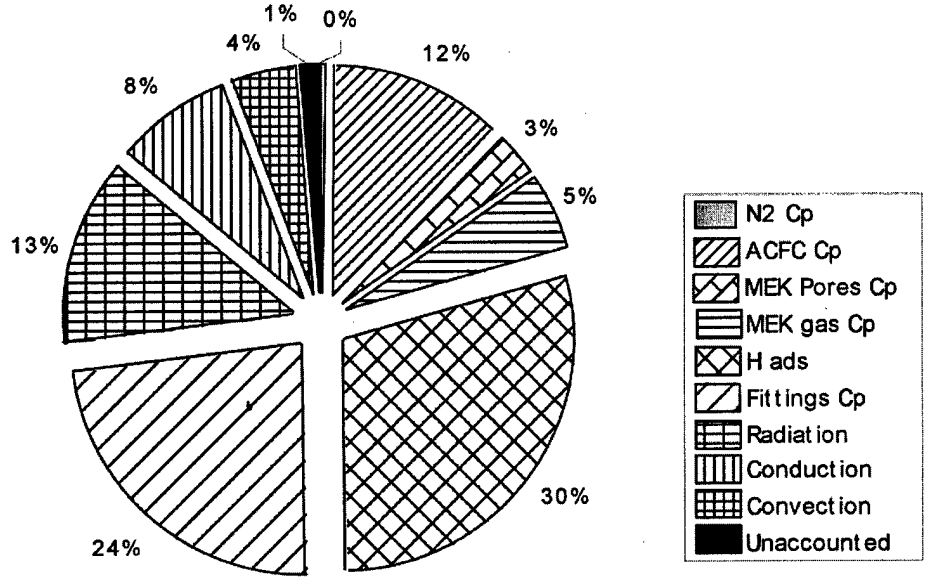

FIGURE 11. Results for inner energy balance around ACFC cartridges. Closure is within −7% of the measured electrical energy input.

condensation begins to occur supports the accuracy of the modeled temperature results. If the measured temperature profile were accurate, then the mass of adsorbate remaining in the ACFC would exceed the equilibrium mass as predicted by the DR equation in mid-cycle.

Panels C and D of Figure 14 show the remaining adsorbed MEK in the ACFC and the MEK vapor concentration in the annulus, respectively. Of the original adsorbed mass of MEK, 70% is recovered as condensate (panel A), 27% is retained in the ACFC (panel C), and the remaining 3% is released as a vapor from the process. These values agree to within 5% of the idealized graphical representation of the desorption using the isotherm plots as shown in Figure 4.

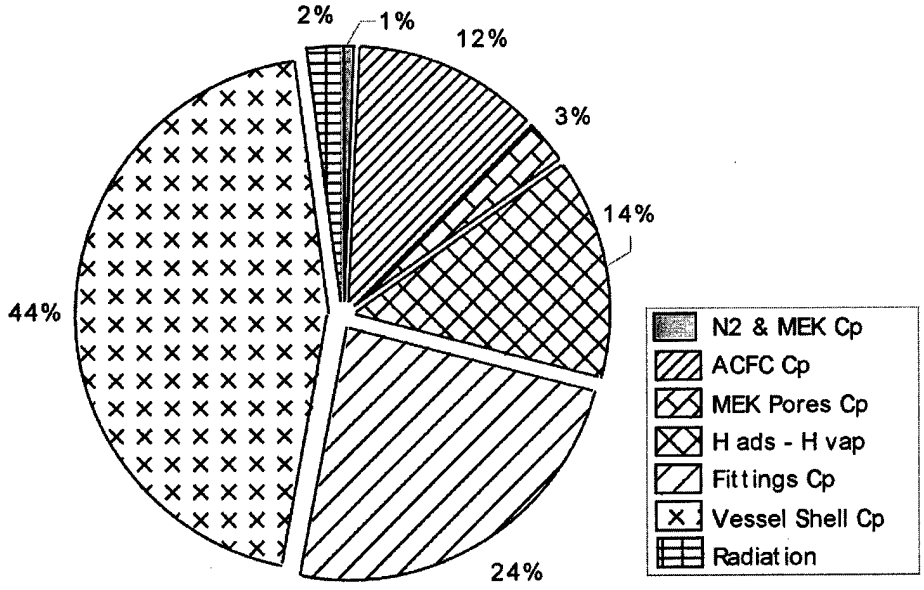

FIGURE 12. Results for outer energy balance around entire adsorber. Closure over-prediction is within +2% of the measured electrical energy input.

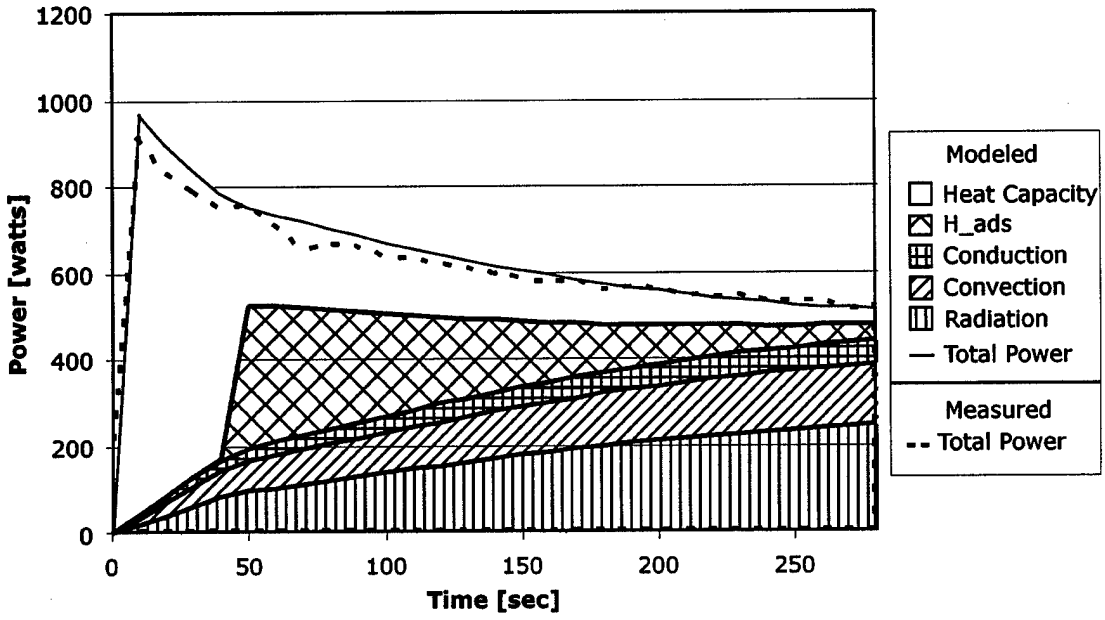

FIGURE 13. Temporal variability of modeled and measured energy terms for desorption of MEK.

Desorption tests were also performed with other relevant adsorbates to demonstrate the generality of the methodology described above. Results from separate tests during which the ACFC was saturated with acetone at 1000 ppmv and methyl propyl ketone (MPK) at 250 ppmv are shown in Figure 15, panels A and B, respectively. The modeled recovery of condensate agrees well to the measured recovery results. Temperature profiles exhibit the same general structures as those obtained for the MEK test. Similar results are obtained with methyl isobutyl ketone and toluene. Tests with select power application algorithms and MEK, acetone, and MPK adsorbate loadings at vapor concentrations ranging between 250 and 1000 ppmv had mean absolute errors <6.7% and R^2 >0.998 (*13*).

For compounds with greater saturation vapor pressures than MEK, the model assumptions begin to break down. The vessel shell at ambient temperature does not provide sufficient cooling to completely condense these compounds. Desorption of acetone at lower power levels resulted in lower recovery (by 40%) than that predicted by the model. Desorption of methylene chloride resulted in ~10% condensate recovery of the adsorbed mass, and rapid venting of excess vapor from the vessel was observed (*23*). Auxiliary cooling of low flow rate effluent from the adsorber may be needed for compounds with saturation vapor pressures >0.2 atm at 20 °C.

Simulations. Simulations of select power application algorithms allow comparison of results for constant current, power, and voltage scenarios in Figure 16A. All three scenarios use inputs described in Table 1 unless specified otherwise. Simulations consumed 180 kJ ± 5% per regeneration cycle. Constant current yields the largest initial power deposition and the sharpest profile for condensate recovery and will thus have the greatest potential for energy optimization.

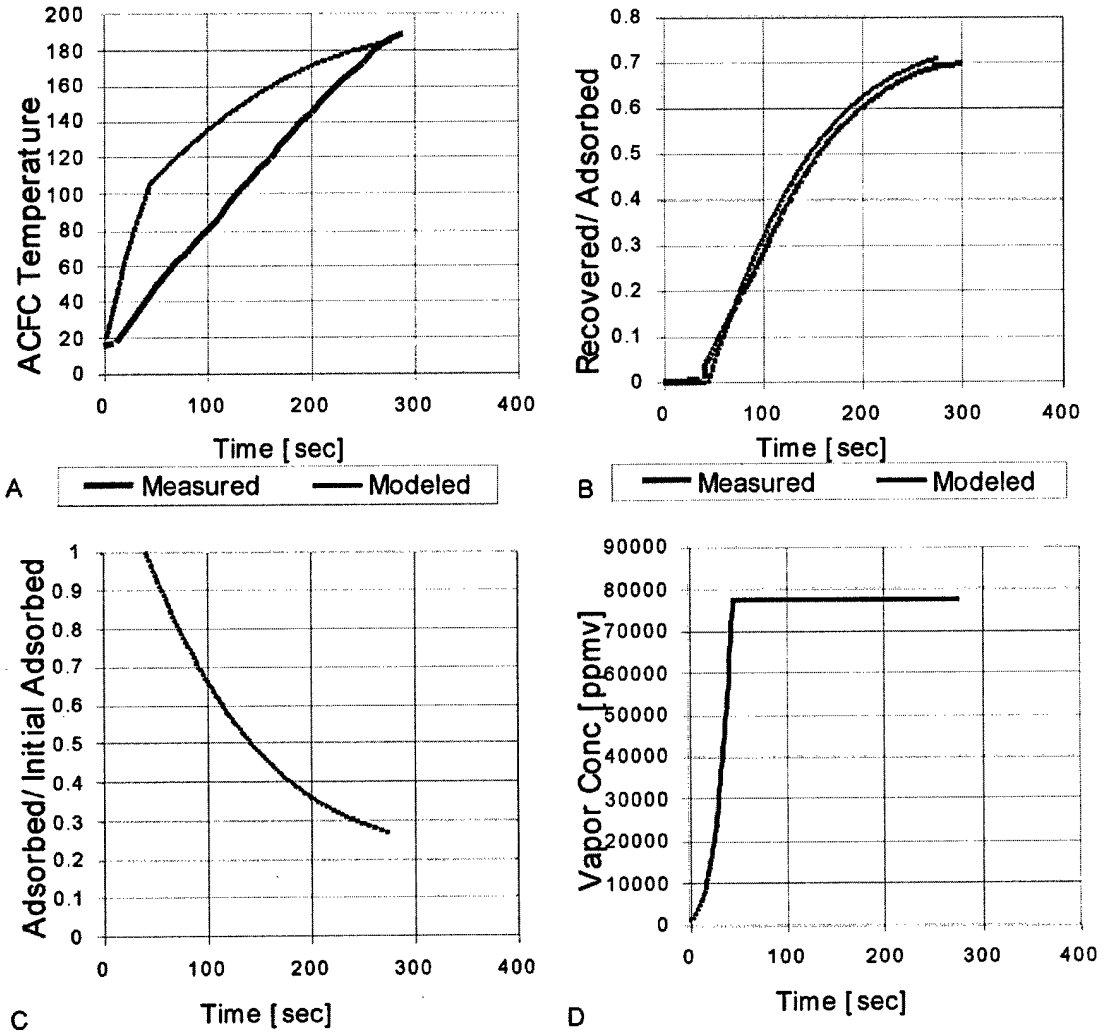

FIGURE 14. Comparison of modeled and measured results during desorption of MEK with an initial loading of 1000 ppmv.

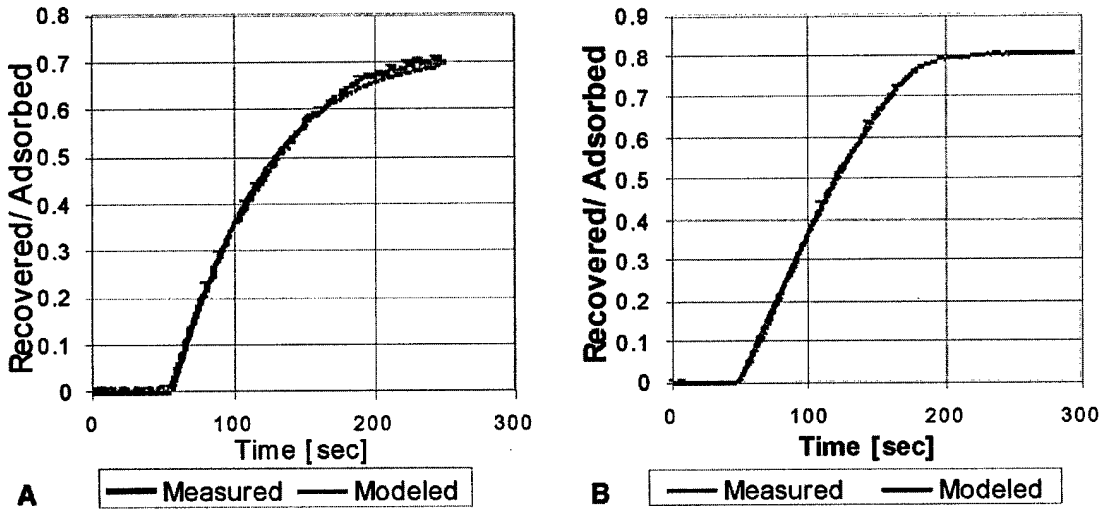

FIGURE 15. Comparison of modeled and measured cumulative condensate during desorption. ACFC was saturated with acetone at 1000 ppmv (A) and MPK at 250 ppmv (B).

Figure 16B shows power consumption for the constant current and constant voltage scenarios. At constant voltage, the total power consumption is the same, but more power is delivered later in the process when the temperature is elevated and energy losses are greater. In addition, with constant voltage, the peak current is more than 50% higher,

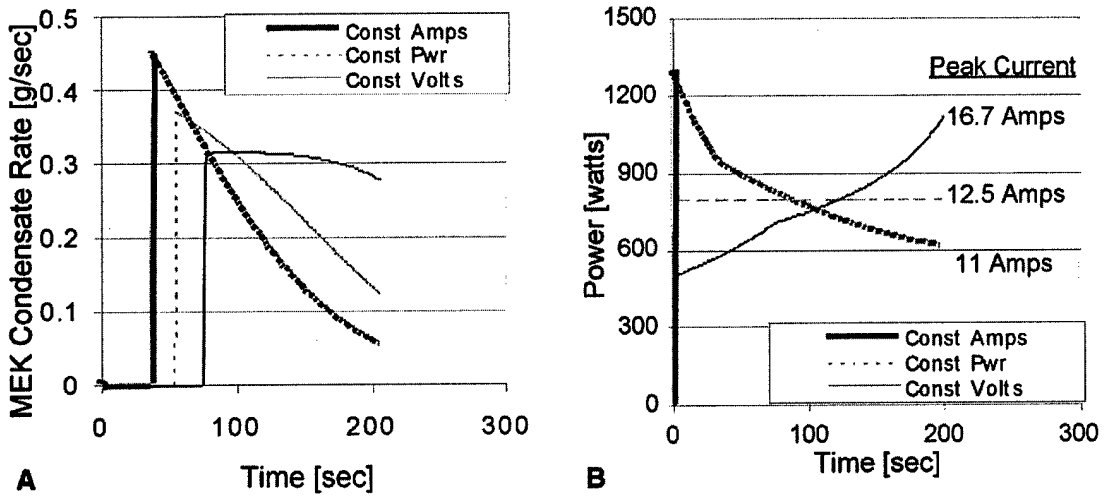

FIGURE 16. Comparison of modeled desorption rates (A) and power profiles (B) for power application algorithms of constant current, constant power, and constant voltage.

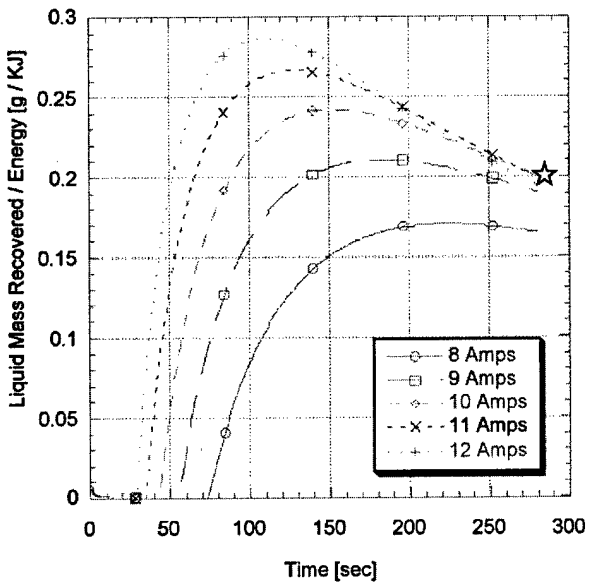

FIGURE 17. Simulated desorption results for energy efficiency with select current values.

requiring higher current capacity circuitry. A variable-voltage power supply with temperature feedback allowing the application of a constant current is preferred.

Simulations for select constant current levels give insight into the energy efficiency of electrothermal desorption (Figure 17). Higher energy input rates increase energy efficiency. Termination of the desorption cycle at 200 °C as used for the experiments is beyond the optimal shutoff temperature for energy efficiency, which is about 160 °C. Although a lower maximum temperature is more energy efficient, it requires more adsorbent and a larger vessel to treat the same volume of gas and therefore might result in a higher overall cost of operation. A more detailed economic evaluation is needed to determine optimum operating parameters for the system (*24*).

Acknowledgments

This study was supported by the U.S. Army Construction Engineering Research Laboratory (CERL); the U.S. Air Force PALACE Knight program; the U.S. Air Force Research Laboratory; the University of Illinois; and the Chemical Engineering Science Laboratory–CNRS, ENSIC, Nancy, France.

Literature Cited

(1) Yang, R. T. *Gas Separation by Adsorption Processes*; Brenner, H., Ed.; Butterworth Publishers: Stoneham, MA, 1987; pp 352.

(2) Bathen, D.; Schmidt-Traub, H.; Stube, J. Experimenteller vorgleich verschiedener thermischer desorptionsverfahren zur losungsmittel ruckgewinnung. *Chem. Ing. Tech.* **1997**, *69*, 132–134.

(3) Petkovska, M.; Mitrovic, M. One-dimensional, nonadiabatic, microscopic model of electrothermal desorption process dynamics. *Chem. Eng. Res. Des.* **1994**, *72* (A6), 713–722.

(4) Sullivan, P. D.; Rood, M. J.; Dombrowski, K. D.; Hay K. J. Capture and recovery of organic compounds using adsorption and electrothermal regeneration. *J. Environ. Eng.* **2004**, *130* (3), 258–267.

(5) Subrenat, A.; Le Cloirec, P. Adsorption onto activated carbon cloths and electrothermal regeneration: its potential industrial applications. *J. Environ. Eng.* **2004**, *130* (3), 249–257.

(6) Subrenat, A.; Baleo, J. N.; et al. Electrical behaviour of activated carbon cloth heated by the joule effect: desorption application. *Carbon* **2001**, *39*, 707–716.

(7) Yu, F. D.; Lou, L. A.; Grevillot, G. Electrothermal desorption using Joule effect on an activated carbon monolith. *J. Environ. Eng.* **2004**, *130* (3), 242–248.

(8) Lordgooei, M. Adsorption thermodynamics and mass transfer of toxic volatile organic compounds in activated-carbon fiber cloth for air pollution control. In *Environmental Engineering in Civil Engineering*; University of Illinois at Urbana–Champaign: Urbana-Champaign, 1999; p 184.

(9) Sullivan, P. D.; Rood, M. J.; Hay, K. J.; Qi, S. Adsorption and electrothermal desorption of hazardous organic vapors. *J. Environ. Eng.* **2001**, *127* (3), 217–223.

(10) Sullivan, P. D.; Rood, M. J.; Hay, K. J. Volatile organic compound recovery using activated-carbon fiber-cloth with rapid electrothermal desorption. In *Proceedings of A&WMA 93rd Annual Meeting & Exhibition*, Salt Lake City, 2000; Paper 629.

(11) Hayes, J. S., Jr.; Sakai, N. Cyclohexanone recovery on activated carbon fiber. In *Proceedings of A&WMA 94th Annual Meeting & Exhibition*, Orlando, FL, 2001; Paper 460.

(12) Zerbonia, R. A.; Brockmann, C. M.; Peterson, P. R.; Housley, D. Carbon bed fires and the use of carbon canisters for air emissions control on fixed-roof tanks. In *Proceedings of A&WMA 93rd Annual Meeting & Exhibition*, Salt Lake City, 2000; Paper 256.

(13) Sullivan, P. D. Organic vapor recovery using activated carbon fiber cloth and electrothermal desorption. In *Environmental Engineering in Civil Engineering*; University of Illinois at Urbana–Champaign: Urbana-Champaign, 2003; p 117.

(14) Lo, S.-Y. Characterization of the chemical, physical, thermal and electrical properties of a series of activated carbon fiber cloths. In *Environmental Engineering in Civil Engineering*; University of Illinois at Urbana–Champaign: Urbana–Champaign, 2002; p 110.

(15) Ramirez D.; Lehmann, C. M. B.; Rood, M. J.; Hay, K. J. Adsorption of organic vapors on tire, coal and phenol derived activated carbons. In *Proceedings of A&WMA 94th Annual Meeting & Exhibition*, Salt Lake City, 2001; Paper 456.
(16) Cal, M. P.; Larson, S. M.; Rood, M. J. Experimental and modeled results describing the adsorption of acetone and benzene onto activated carbon-fibers. *Environ. Prog.* **1994**, *13* (1), 26−30.
(17) Ramirez, D.; Sullivan, P. D.; Rood, M. J.; Hay, K. J. Equilibrium adsorption of organic vapors on phenol-, tire- and coal-derived activated carbons. *J. Environ. Eng.* **2004**, *130* (3), 231−241.
(18) Reid, R. C.; Prausnitz, J. M.; Poling, B. E. *The Properties of Gases & Liquids*, 4th ed.; Sun, B., Fleck, G. H., Eds.; McGraw-Hill: New York, 1987; p 741.
(19) Salinas, M. J.; Price, D. W.; Schmidt, P. D. VOC recovery using microwave regeneration of adsorbents: pilot-column studies. In *Proceedings of A&WMA 92nd Annual Meeting & Exhibition*, St. Louis, MO, 1999; Paper 356.
(20) Incropera, F. P.; Dewitt, D. P. *Fundamentals of Heat Transfer*; John Wiley & Sons: New York, 1981; p 819.
(21) Ramirez D.; Lehmann, C. M. B.; Sullivan, P. D.; Rood, M. J. Adsorption of methyl ethyl ketone and acetone by tire-derived activated carbon and activated carbon fiber cloth. In *Proceedings of A&WMA 93rd Annual Meeting & Exhibition*, Salt Lake City, 2000; Paper 466.
(22) Lide, D. R., Ed. *Handbook of Chemistry and Physics*, 74th ed.; CRC Press: Boca Raton, FL, 1993.
(23) Dombrowski, K.; Lehmann, C. M. B.; Sullivan, P. D.; Ramirez, D.; Rood, M. J.; Hay, K. J. Solvent recovery and energy efficiency during electric regeneration of an ACF adsorber. *J. Environ. Eng.* **2004**, *130* (3), 268−275.
(24) Kaldate, A.; Thurston, D.; Rood, M. J.; Emamipour, H. Development of cost-effective adsorption-electrothermal desorption system using activated carbon fiber cloths. In *Proceedings of 96th Annual Meeting & Exhibition of the Air & Waste Management Association*, San Diego, CA, 2003; Paper 69834.

Received for review September 24, 2003. Accepted June 14, 2004.

ES0306415